Rhythmic dynamics of associative memory processing in the rodent Dentate Gyrus

Chris Heyman

Neural Crossroads Laboratory, Cognitive Science Dept. UCSD

Supervisors: MIA BORZELLO, PH.D. STUDENT & DR. LARA MARIA RANGEL, PH.D.

June 11, 2021

Abstract

While we know much about which regions are important for associative memory, we know little about the processing that occurs within these regions which enable their contribution to processing associations. We investigated markers of circuit dynamics to determine how associative memory processing may be gated by engagement of specific circuits in the Dentate Gyrus. We found shifts in the rhythms present in local field potentials of the Dentate Gyrus during cue intervals corresponding to associative memory task performance. Additionally, during cue intervals, putative granule cells fired in coherence with specific phases of identified rhythms significantly more in trials where the animal made a correct association. However, these neurons did not exhibit firing rate changes in an outcome-predictive manner, suggesting that their engagement in specific rhythmic circuits is more salient for associative memory processing than their gross activity.

Introduction

Memory allows animals to learn from repeated experience. By repeatedly associating a unique combination of stimuli with an outcome, animals can build a memory which allows them to form accurate predictions. This associative form of memory is crucial not only for tasks of our everyday life, but also for the survival of animals in the wild. Consider the daily life of a forest rat. It's critical for such an animal to associate and recall sensory aspects or objects--such as a particular smell or light--at a specific spatial location, which predicts whether a nearby tree will have shed its delicious fruit or will be surrounded by dangerous predators. The hippocampus receives sensory inputs from many structures and is widely known to be important for these types of associative memories. Primary hippocampal subregions such as the Dentate Gyrus (DG), cornu ammonis 1 (CA1), cornu ammonis 3 (cornu ammonis 3), and subiculum all receive independent inputs from sensory regions such as the medial entorhinal cortex (MEC) and lateral entorhinal cortex (LEC), which respectively carry primarily spatial and non-spatial information(Amaral et al., 2017; Fernández-Ruiz & Oliva, 2016; E.T. Rolls, 1996; O'Reilly & Rudy, 2001; Eichenbaum, 2015) . The convergence of these sensory inputs could enable processing to occur in these hippocampal subregions which are necessary for formation, integration, and/or recollection of associative memories. Results from previous studies involving lesions, pharmacological blockades, and electrophysiology suggest the potential for a unique role of the DG in associative memory.

Animal studies have shown that disruption of synapses at the dorsal DG result in: attenuated performance on tasks which require a rat to associate different contextual representations of the spatial environment with different odors to receive a reward (Morris et al., 2013), less novelty exploration in object-context recognition tasks where the spatial context cues changed colors (Dees and Kesner, 2013), and diminished performance on pattern separation tasks for shades of grey (Kesner, 2018). In rats, pharmacological blockade of long term potentiation (LTP) along only the perforant path from LEC to the dorsal DG has been shown to result in significantly substandard performance in novel object detection tasks. Blockades of LTP in either the perforant path from MEC or LEC resulted in diminished performance in spatial change detection. Furthermore, blocking LTP along either path to CA3 resulted in behavioral failures in both the spatial and object-based tasks (Hunsaker et al., 2007). Importantly, CA3 has inputs directly from both the perforant paths and from DG, but only the perforant paths were blocked. This may imply that neither DG or CA3 alone is sufficient to complete tasks that require recollection and comparison of a previous environment. Further, the dentate gyrus may process incoming sensory information to form highly distinct representations of the environment which aid in tasks which involve understanding the relationships between two otherwise unrelated items. A distinct form of associative memory processing in the dentate gyrus could be enabled by the relatively idiosyncratic connections between it's different cell types and their physiological properties.

In the DG, an extensive network of highly target specific inhibitory interneurons give rise to widespread temporal windows of hyperpolarization, drastically increasing thresholds for action potentials (Buckmaster & Schwartzkroin, 1995), and thereby differentially limiting communication along the complex sets of both inter-DG and intra-DG connections to tight temporal windows of momentary reprieve yielded by refractory periods within the interneuron network. Given the multitude of connections between cells of the DG and the ability of these cells' physiological properties to be altered (through mechanisms including, but not limited to, neuroplasticity), the time course and targets of the DG networks inhibitory currents may be actively modulated to allow dynamic engagement and disengagement of many functional circuits. The exchange of charged ions through a neuron's cell membrane marks its activity. This physiological property allows measures of summed extracellular currents -- such as the local field potential (LFP) -- , to be used as a high level view into network activity (Cannon et al., 2014). Assessment of the development of rhythmic components of the LFP as they relate to the development of cue intervals of associative memory tasks allows for a more precise view into how DG circuits interact and change in a manner that may be crucial for processing. Engagement or disengagement of specific circuits may be crucial for memory formation, integration, recollection, and propagation for use in other brain regions. Indeed, these rhythmic dynamics have been shown to be related to successful memory recall and task performance in previous studies investigating other regions of the hippocampal system (Rangel et al, 2015), within the

DG itself (Rangel et al, 2016), and to enable functional connections between regions (Kopell et al., 2000; Bibbig et al., 2002; Pinto et al., 2003).

The above outlined view of oscillatory dynamics implies that information containing neuronal signals or spikes may only have downstream effects when integrated into specific phases of rhythmic components of the LFP corresponding to unique neural circuit engagement. Previous work has shown that temporal organization of action potentials into different phases of rhythms may act to modulate the relay of encoded information to local circuits through compression of cell firing into temporal windows of regional depolarization or hyperpolarization (Kopell et al, 2010; Buzsáki, 2010). A neuron's temporal engagement in the rhythmic electrical oscillations observable in connected brain regions could be important for modulating that neuron’s interactions between cells in the same population and cells in more distant connected circuits. We aimed to investigate how performance on associative memory tasks correlated with these proxies for circuit and cell-circuit interactions to gain insight to the understudied functional anatomy of the DG which is crucial for associative memory.

Macro level shifts in rhythms and micro level shifts in how individual cells interact with these rhythms may reveal a hidden neural code used to bind multiple sets of incoming sensory information and associate it with an outcome. By examining rhythmic dynamics in animals during an associative memory task, we can gain insight

into how different rhythms may engage different macro and micro level circuits important for processing learned cues to predict an outcome.

In this work we identified frequency bands of rhythmic activity which shift during intervals containing --potentially conjunctive-- cues for associate memories. We found that a decrease in theta (5-10Hz) and beta (15-35Hz) amplitude during the cue interval was predictive of improved associative memory task performance. We then analyzed how each cells' firing preference for a specific phase of each rhythm found to develop during cue intervals predicts subsequent associative memory task performance. We found cell entrainment in specific rhythms during the cue interval can predict performance in the following associative memory task. Specifically, a significantly greater population of putative granule cells (cells with <3Hz average firing rate), exhibit significant entrainment to theta (5-10Hz), beta (15-35Hz), low gamma (35-50hz) or very high gamma (75-115Hz) rhythms, only during behavioral outcomes indicative of successful associative memory processing. Importantly, these cells did not exhibit significant differences in firing rate during the cue interval between the associative memory task outcomes. Building on previous work, computational models, and our results, we propose that during learning of associations, repeated stimulation of sensory inputs to granule cells induces changes in synaptic strength at the entorhinal-granule cells synapse, which in turn leads to functional changes in the circuitry of the DG when associative cues reappear. These functional changes manifest as decreases in theta and very high gamma rhythmic contribution to the local field

potential, which may be reflective of disinhibition of circuits needed for processing associative cues. Additional functional changes are observable in the emergence of spike phase relationships between putative granule cells and theta, beta, low gamma, and very high gamma rhythmic profiles. Importantly, all of these functional changes appear to be changes in when, rather than how often, putative granule cells fire, reflecting that circuit engagement may be more important than raw firing rate.

Finally, these results give plausibility to a new conjunctive encoding hypothesis. If convergence of multiple sensory signals onto single granule cells could result in the strongest functional changes at the entorhinal-granule synapse and thus downstream effects, a neural code for conjunctions could be hidden in temporal patterns of granule cell circuit engagement.The next steps in validating these dynamics as markers of a conjunctive neural code will involve further analysis of what specific cue-related sensory information each one of these putative granule cells' spikes may carry.

Methods: Data collection (Section adapted from previous writing by Dr. Lara Rangel. Data collected in 2016 by Dr. Lara Rangel, Pamela Riviere, and colleagues at the Center for Memory and Brain, Boston University. Adapted from Dr. Lara Rangel)

All animal procedures were performed in accordance with NIH and Boston University Institutional Animal Care and Use Committee guidelines. Subjects were six male Long-Evans rats kept on food and water restriction until they reached 85-90% of *ad libitum* body weight. Weights ranged from 500-600g.

Behavioral Apparatus: Rats were first exposed to the testing apparatus: a two-arm maze constructed of black plastic (Figure S1). Each 45-cm arm extended from opposite ends of a 30-cm central chamber. The central chamber consisted of 20-cm high walls and two pairs of doors, one black and one clear, that opened onto either arm. All doors could be independently raised and lowered by electric actuators. The end of each arm contained a widened area with two circular odor ports (Figure S1, inset), into which an odorant could be released by opening an air solenoid. Odorants were delivered by air flowing over vials of oil-based scents, previously characterized as differentiable by the rats. 12 odors were used, some of which were natural scents (maple, cedar, spearmint, strawberry, sweet orange, mango, lemon) while the others were chemical odorants (2-phenylpropionaldehyde, allyl-a-ionone, cis-3-hexen-1-ol, guaiacol, isoamyl acetate). Each port also contained a vacuum, which removed the odorant after release to prevent cross-contamination of odors between trials. Below each odor port was a tray with a well, into which water could be released to reward successful performance. Throughout the maze there were LED sensors to verify rat movement: two along the length of each arm, one in each odor port, one in each water well, and two in the central chamber. LED sensors in each odor port and water well also acted to record stimulus onset and reward onset, respectively. All maze functions

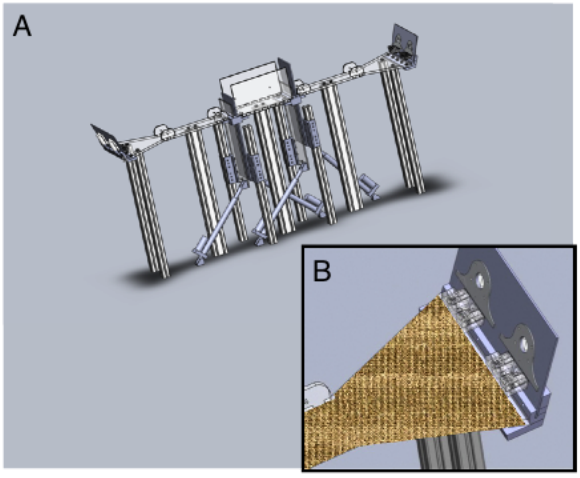

Figure S1. Automated two-arm maze. (A) CAD drawing of automated two-arm maze. Each arm is connected to a central chamber of high walls and two pairs of a clear and opaque door. Independent electronic actuators control the doors. (B) Close-up view of the end of one arm with a context wrap placed over the structure. Two odor ports and water reward trays are located at the end of each arm.

were controlled via a computer by MATLAB programs.

Behavioral Training: Each rat underwent a behavioral shaping process to first poke its snout in an odor port and then increase the length of each poke. Rats received training sessions in which initially 100ms pokes elicited a water reward. The poke criterion increased by 100 ms for each poke of sufficient length and dropped by 100 ms for every two successive unsuccessful pokes until rats learned to consistently poke for 1.5 seconds. During this process, rats only had access to one port at a time and received equal exposure to all four ports on the maze.

Following poke training, each rat was taught to discriminate between two odors of an odor pair. During early discrimination sessions, two different context overlays made of distinct materials were placed over each side of the maze, and the rat was given access to one arm of the maze at a time. Rats alternated between arms in blocks of 20 trials during initial training, followed by blocks of 10 trials upon improved performance. Ultimately, arms switched in a pseudorandom, counterbalanced fashion in all later sessions.

Full Task: During each trial, each of the odors would be presented on one side of the maze, one odor in each of the two ports. Importantly, one odor of the pair was designated as a “correct” odor, and sustaining a poke of 1.5 seconds in the odor port containing this odor resulted in a water reward. The other odor was not rewarded, and a white noise buzz would occur if the rat sustained a poke for 1.5 seconds in that port, after which the rat was required to return to the central chamber before being allowed

to return to poke again. Upon choosing the correct odor and consuming the water reward, rats had to return to the central chamber, after which the doors would raise, and the next trial would begin. The same odor was always correct for that context overlay and side of the maze. The location of the correct odor could switch between the left and right ports each trial, and trials were counterbalanced and pseudorandomized before each session. The roles of the odors were reversed for each arm: the incorrect odor from the first arm was the correct odor on the second arm and vice versa. Each rat underwent 80 trials a day until reaching a criterion of 80% accuracy. With this same final paradigm, rats were trained on one four-odor set (two pairs) for three to five weeks before surgery and two subsequent four-odor sets for three to five weeks each after surgery. Each four-odor set contained distinct odors and context overlays. Recordings were collected as rats performed a 96-trial session of the two post-surgery odor sets (24 trials per odor pair).

Hyperdrive Implantation Surgery: Following training, each rat was surgically implanted with a hyperdrive containing 24 microdrives, each with an independently drivable tetrode. Each tetrode was composed of four strands of 0.0005” (12 μm) Nickel-Chrome wire (Sandvik, Stockholm, Sweden), gold-plated to reduce impedance to 200-250kOhms at 100Hz. The implant site was located over the right dorsal hippocampus (anterior-posterior [AP] = -4.0 mm; medial-lateral [ML] = 2.2 mm), and tetrodes were turned down an initial 1.6 mm into the brain immediately following surgery. After rats received two weeks of rest post-surgery, tetrodes were progressively lowered over the

training period (6-7 weeks) to the pyramidal cell layer of CA1 and granule cell layer DG (CA1: dorsal-ventral [DV] = 1.9 mm; DG: DV = 2.7 mm). Tetrode locations were confirmed by LFP characteristics including sharp-wave ripples for CA1 and dentate spikes for DG, and final locations were confirmed by tissue slide analysis.

Neural Recordings: Recording sessions consisted of a block of 48 trials of odor set 1 (24 with the first odor pair; 24 with the second pair) followed by 48 trials of odor set 2, in similar fashion. Additionally, all conditions were counterbalanced and pseudorandomized within each 24-trial block, being pseudorandomized before each session. Before and after recording sessions, the rat was placed on a separate platform for five minutes to serve as a baseline to compare activity during behavior. Signals were amplified by a preamplifier 20x and amplified again to 4,000-6,000x (Plexon, Dallas, TX), with a band-pass filter of 600-6,000 Hz to digitally isolate spikes. Signals were globally referenced to a wire above the cerebellum, as well as locally referenced to a wire with low activity. LFPs were digitally isolated with a band-pass filter from 1-500 Hz (OmniPlex, Plexon). Throughout the session, the rat's location was recorded via digital video and tracking software (CinePlex, Plexon) that monitored the motion of two LEDs mounted at the top of the rat's hyperdrive. Along with behavior data from the LED sensors, this data was timestamped and synchronized with the LFP and spiking data, all of which was stored offline for later analysis.. Single units were identified in OfflineSorter (Plexon), comparing features including peak and valley voltage amplitudes, total peak-to-valley amplitudes, and principal components. 15 recording

sessions were performed over the course of 3-5 weeks from each rat, with rats resting on days between sessions.

Methods: Analysis (Conducted by Chris Heyman with assistance from Dr. Lara Rangel and members of Neural Crossroads Laboratory, University of California, San Diego)

Inclusion criteria: LFP and single unit data originating from electrodes in the dentate gyrus were filtered to ensure only data from days in which rats completed at least 80% of scheduled trials and an average of 75% task accuracy for each 4-odor block were processed.

General segmentation of Data: Data from each day and trial which met the above criteria were passed through a function which partitioned data by its temporal correspondence to the rat's behavior (for example: correct, incorrect, or self-corrected, or correct rejection).

Spectrograms: Data sets passing the above criteria from were decomposed and segmented into each respective interval (ie 1.5 seconds nose poke of a correct trial) via Fourier transforms and the multi-taper method from the Chronux open source MATLAB toolbox (available at: http://chronux.org/) (Mitra and Bokil, 2008). The mean data for each interval which occurred on a given day for a given rat was taken, then normalized by iteratively dividing the mean data collected for the corresponding inter-trial interval (when the rat was in the center chamber of the behavioral apparatus). Then the base 10 log value of results was taken to adjust the scale of

amplitudes before taking the mean across all normalized data. The resultant data was then plotted as a spectrogram. These spectrograms were then visually analyzed to reveal frequency bands of interest for further analyses.

Alterations in frequency band development during odor sampling for rhythms of interest: Whole LFP datasets which met inclusion criteria were passed through third order butterworth filters banded by frequencies identified through methods outlined in *spectrograms,* prior to interval based segmentation listed above, to avoid edging effects which result from segmented processing. For each interval and condition of interest, we binned the signal into 6 250ms bins following the nose poke. A two factor repeated measures ANOVA was run to test for significant differences across bins and conditions in a given interval. This allowed us to quantitatively determine if the signals observable in the spectrogram were in-fact dynamically changing and if they differed in a manner correlated with task performance.

Spike Phase Relationships: A Rayleigh statistic was used to determine if the mean of each cell's spiking activity was significantly clustered to the corresponding instantaneous phase of a given rhythm of interest during the odor sampling epoch. As cells behaved differently depending on the context, they were considered as independent cells in each context for all single cell related analysis.

Behavioral spike phase relationships: For each cell with significant spike phase relationshapes ($P<0.05$) to a given rhythm of interest, we categorized them into depending on their spike phase relationships being significant during only correct,

only incorrect, or during both behavioral outcomes. We then assessed if there were significant differences ($P<.05$) across the categories using a chi-squared test. Post-Hoc chi squared tests were then used to compare pairwise for each category with a bonferroni adjusted P-value of 0.0167.

Session Average Firing Rate: On each day which met above criteria, the total number of spikes from each DG cell was pooled and divided by the corresponding total time length of the session. These session average firing rates were then used as criteria for categorizing cells into functional types which aligned with properties of cell types in the region (i.e. cells with average firing rate <3Hz corresponding to putative granule cells).

Interval Average Firing Rate: First, we established which DG cells which were within a specified session average firing rate range and had a significant spike phase preference (as quantified by the Rayleigh Statistic) to a given rhythm of interest during the odor sampling interval. As cells behaved differently depending on the context, they were considered as independent cells in each context. This data was then segmented to find which cells had significant spike phase relationships during correct or incorrect outcomes. We assessed how the average firing rate per cell during the interval differed across outcomes. To do this, we examined the average number of spikes these cells had per odor sampling interval, in which they exhibited a significant spike phase relationship for at least one outcome. If a cell had significant spikes for one outcome but not another its mean interval firing rate was still calculated. If a cell had significant

spikes for one outcome but did not fire for another, it's mean interval firing rate for that outcome was zero. If a cell had significant results for both outcomes, it's mean interval firing rate was calculated for both.

Testing for differences in Interval firing rate between outcomes: For each rhythm, DG cells which fell into a session average firing rate range and had a significant spike phase preference during correct, incorrect, or both trials of interest were assessed for differences in firing rates during the intervals investigated which could bias the Rayleigh statistic. Histograms were plotted and the Anderson-Darling test was employed to assess normality of data. As at least one outcome in each pair of outcomes did not have a normal distribution, the Wilcoxon Signed Rank test was used to test for difference in average firing rates between each condition, at each rhythm.

Results

Both single cell and local field of potential activity of the DG was analyzed to assess the development of signals during the cue intervals, and how these signals related to recalling learned sensory cues to gain a reward. From a total of 229 recorded cells in the dentate gyrus, 190 were identified as putative granule cells (session average firing rate <3Hz) and 27 were identified as putative inhibitory cells (session average firing rate >6Hz).

Spectrogram show distinct rhythmic activity during cues

We found that during the cue (odor sampling) interval, prior to reward, several frequency bands changed their contribution to the local field potential. We observed a shift to decreased contributions by theta (5-10Hz) and very high gamma (75-115Hz) following the initiation of an odor sampling interval. Beta (15-35Hz), low gamma (35-50Hz), and high gamma (50-70Hz) exhibited a shift to increased contributions to the local field potential in the same interval (Fig. 1a).

The signals for each rhythm of interest appear to return to baseline levels following cessation of the cue then increase again during reward consumption (Fig. 1b). This indicates the signals associated with the cue interval are distinct from those observable from the reward interval.

Two factor repeated measures ANOVAs were used to test for significant differences between the time from initiation of the nose poke, the contribution of an amplitude envelope to a specified frequency band of the spectrogram, and outcome on the associative memory task (Fig. 1c, Fig. 1d). Across six 250ms time bins following the nose poke, we found a significant difference in the development of each rhythm observable in the spectrograms (Table 1a). Additionally, there was a main effect for outcome (correct or incorrect) for both theta (5-10Hz) and very high gamma (75-115Hz) frequency bands (Table 1a). The mean of theta and the mean very high gamma band activity was significantly greater during incorrect outcomes than correct (Table 1a) but

no significant differences were observed between outcomes for each individual time bins for either rhythm (Table 1a; S1).

	Repeated Measures ANOVA $Time_{Bins\ 1\text{-}6}$	Repeated Measures ANOVA $Outcome_{Correct\ vs\ Incorrect}$	Repeated Measures $ANOVA_{time*outcome}$
Theta (5-10Hz) Muachly test of sphericity indicated sphericity was violated for time and outcome with a Greenhouse-Geisser Epsilon of 0.35819 for time, 0.54058 for time*outcome. Thus, we corrected for the sphericity violation by using Greenhouse-Geisser calculation when examining within subject effects.	Uncorrected d.f. = 5, F= 29.98, p<0.00001 Greenhouse-Geisser d.f=1.79094, F=29.98 p<0.00001	d.f. = 1, F= 10.55, p=0.00257	Greenhouse-Geisser d.f.=2.70288, f=0.4500, p=0.69778 n.s.
Beta (15-35Hz)	d.f. = 5, F= 58.92, p<0.00001	d.f. = 1, F=2.082, p~=0.16, n.s.	
Low Gamma (35-50Hz)	d.f. = 5, F= 21.81, p<0.00001	d.f. = 1, F = 2.121, p=0.15, n.s.	
High Gamma (50-70Hz)	d.f. = 5, F= 8.787, p<0.00001	d.f. = 1, F = 0.5947, p=0.45, n.s.	
Very High Gamma (75-115Hz) Muachly test of sphericity indicated sphericity was violated for time and outcome with a Greenhouse-Geisser Epsilon of 0.53628 for time, 0.67994 for time*outcome.	d.f. = 5, F= 35.64, p<0.00001 Greenhouse-Geisser d.f.=2.68141, F=35.64, p<0.00001	d.f. = 1, F = 4.170, p=0.0487	Greenhouse-Geisser d.f.=3.39972, f=1.644, p=0.18 n.s.

Thus we corrected for the sphericity violation by using Greenhouse-Geisser calculation when examining within subject effects.			

Table 1a. **Summarized results for two factor repeated measures ANOVAs conducted at each frequency band, for six 250ms time bins beginning at the initiation of nose poke, between correct and incorrect memory task performance. If there was a significant effect of outcome and time, we also examined time*outcome interactions.**

	Pairwise Bonferroni Test$_{\text{Correct Vs Incorrect}}$
Theta (5-10Hz)	d.f.=35, t=4.8919, p<0.00003, incorrect mean=0.12682, correct mean=0.11778
Very High Gamma (75-115Hz)	d.f.=35, t=3.0544, p=0.00429, incorrect mean=0.04258, correct mean=0.04173

Table 1b. **Pairwise statistics for interactions between shifts in contribution of given rhythms to LFP during cue intervals and associative memory task performance. Mean amplitude for theta and very high gamma were significantly lower for cue intervals which predicted correct associations**

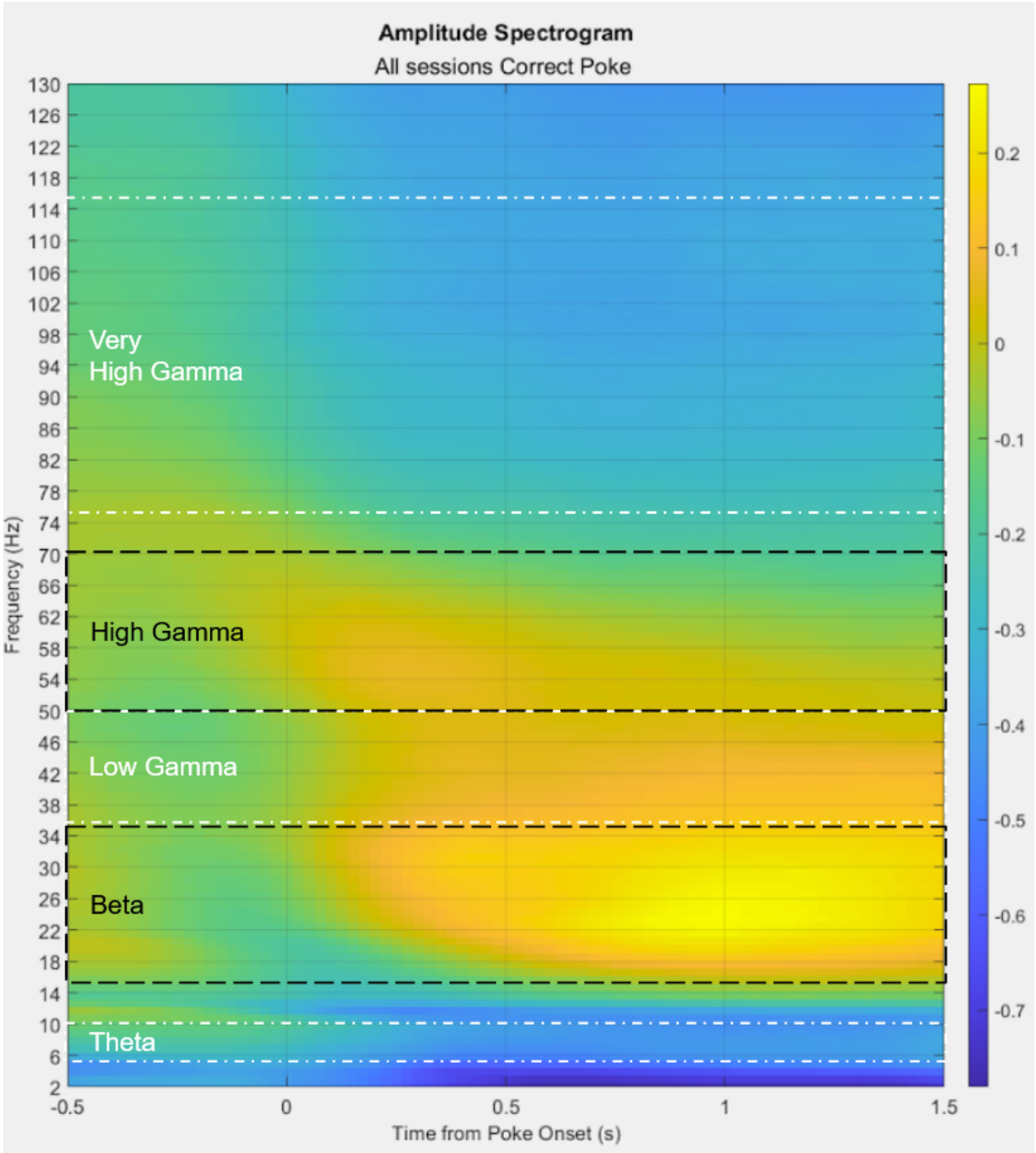

Figure 1a: **Normalized average spectrogram for all correct trials.** Frequency bands identified to fluctuate in response to the initiation of the odor sampling cue interval are boxed and labeled.

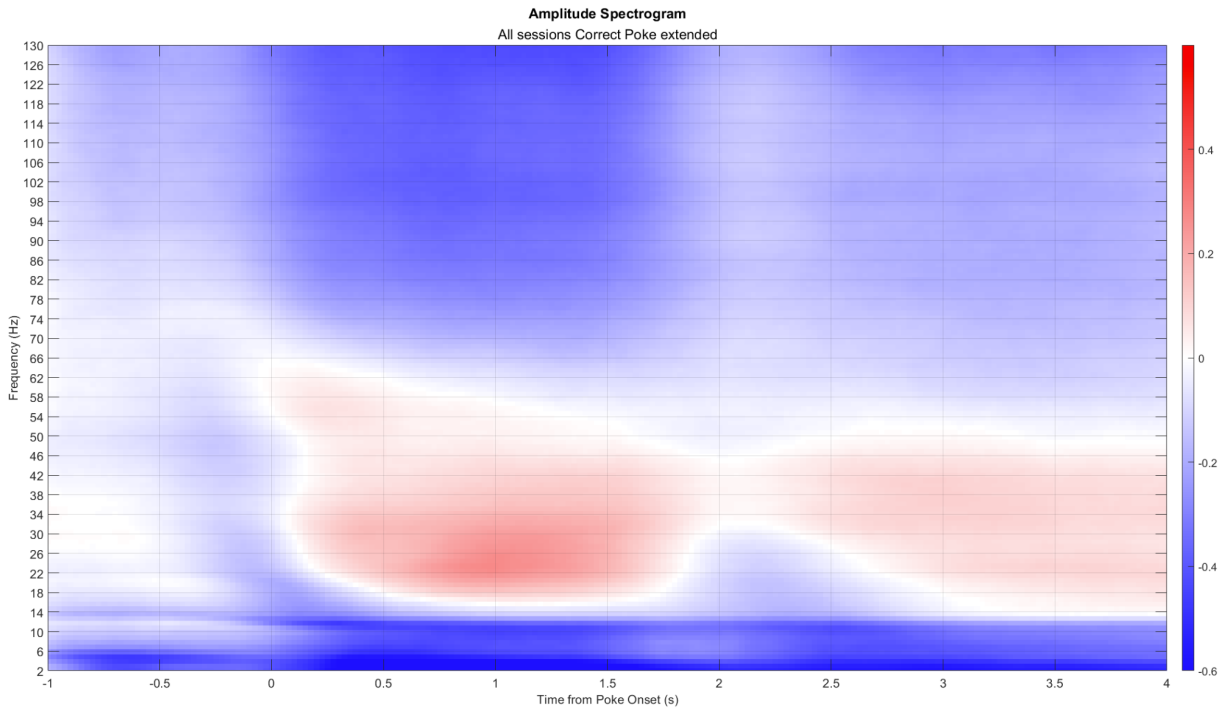

Figure 1b: **Extension of figure 1a with a simplified color axis.** A rat would select one of the odor ports at the 0 second mark by poking its nose in the port. Odor would be released 250ms later, odor sampling would be maintained for 1.5 seconds, then, the rat would begin licking up the reward (on average) at the 1.9 seconds mark.

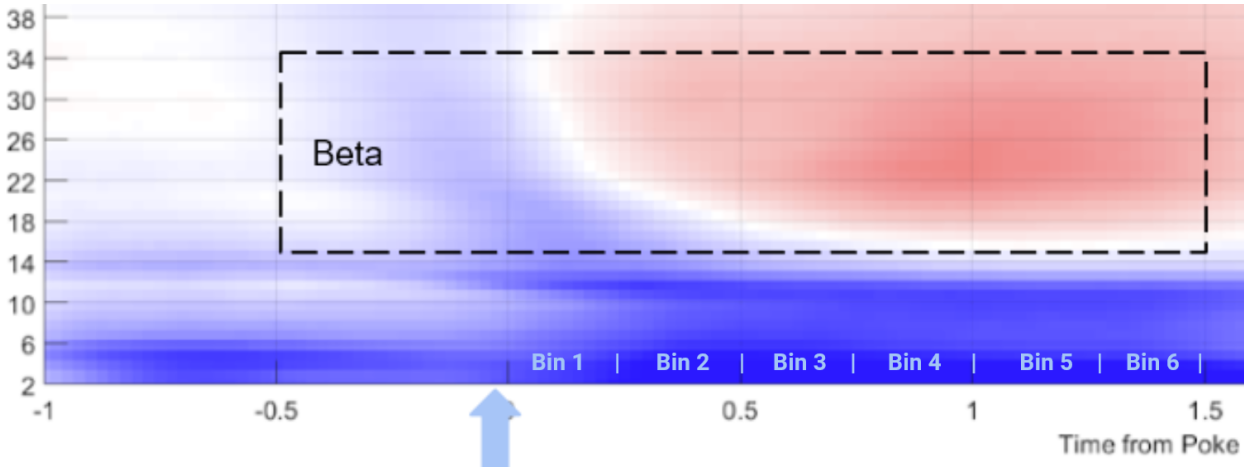

Figure 1c: **Expansion of figure 1b with beta (15-35Hz) outline and time bin overlays.**

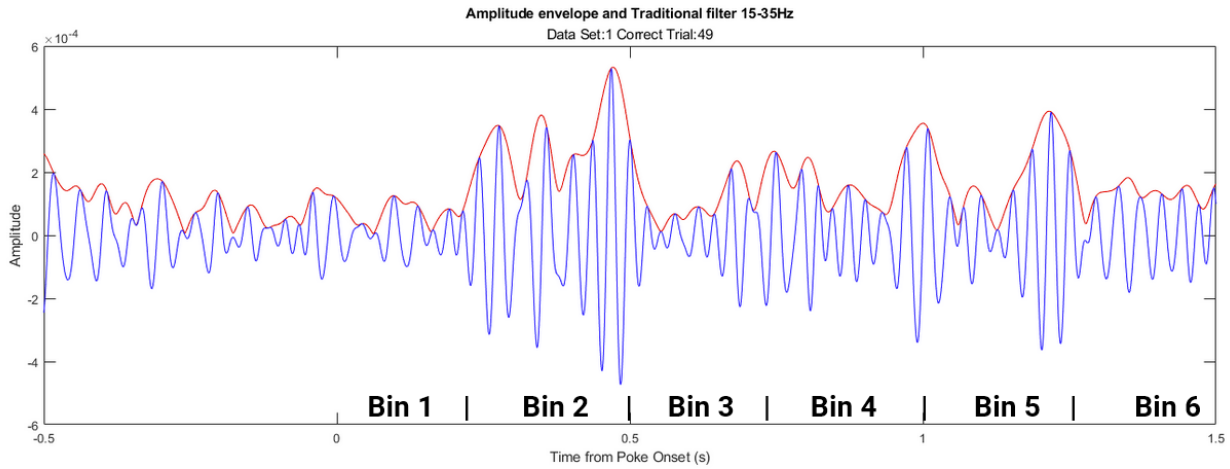

Figure 1d: **Example single trial LFP (blue) and amplitude envelope (red) which contributed to the beta band of the amplitude spectrogram and was used in two factor repeated measures ANOVA.**

Cell spike-phase coherence correlate with task performance

For each rhythm identified to dynamically change over the nose poke interval, we tested if unique engagement of putative granule cells, or unique engagement of putative inhibitory cells, to the specified rhythm during the cue interval was predictive of performance on the associative memory task. Of cells identified to have significant spike phase preferences for each rhythm, we categorized them depending on if these phase preferences were unique to correct, incorrect, or irrespective of trial outcome. For putative granule cells with significant spike phase relationships (N=69, 36 sessions with each half session analyzed separately, 5 rats, see materials and methods) we found coherence predicted correct trial performance for all rhythms excluding high gamma (Fig. 2a; Table 2a). Of putative inhibitory cells with significant spike phase relationships (N=27, 36 sessions with each half session analyzed separately, 5 rats, see materials and methods), we found only beta and high gamma coherence was predictive of performance (Fig 2b; Table2b), though firing rate differences may have skewed these results for the putative inhibitory population for all rhythms of interest besides beta.

	$\chi 2_{\text{correct v incorrect v all}}$	χ2correct v incorrect Bonferoni corrected P value=0.0167	χ2correct v all Bonferoni corrected P value=0.0167	χ2incorrect v all Bonferoni corrected P value=0.0167
Theta (5-10Hz)	(2, N=28) = 24.5, p<0.00001	(1, N=28) = 7, P=0.00815	(1, N=21) = 21, p<0.00001	(1, N=7) = 7, P=0.00815
Beta (15-35Hz)	(2, N= 16)~= 16.6 , P=0.00025	(1, N=15)~= 8.07 , P=0.00451	(1, N=14)~=10.3, P=0.00134	(1, N=3)~=0.334, P~=0.56 N.S.
Low Gamma (35-50Hz)	(2, N=15)~=14.8, P=0.00061	(1, N=14)~= 7.14, P=0.00753	(1, N=13)~= 9.31, P=0.00228	(1, N=3)~= 0.334 , P~= 0.56 N.S.
High Gamma (50-70Hz)	(2, N=8) = 7, P= 0.03019	(1, N=2) = 2, P~=0.16 N.S.	(1, N=6) = 6, P=0.01430	(1, N=2) =2 , P~=0.16 N.S.
Very High Gamma (75-115Hz)	(2, N=42) = 13, P=0.00150	(1, N=34) ~= 7.53, P=0.00606	(1, N=33) ~= 8.76, P=0.00308	(1, N=17) ~= 0.059, P~=0.81 N.S.

Table 2a. **Chi Squared Tests for significant differences in proportion of putative granule cells coherent to a given rhythm for a given condition. (N.S. not significant)**

	$\chi^2_{\text{correct v incorrect v all}}$ P<0.05	$\chi^2_{\text{correct v incorrect}}$ Bonferoni corrected P value=0.0167	$\chi^2_{\text{correct v all}}$ Bonferoni corrected P value=0.0167	$\chi^2_{\text{incorrect v all}}$ Bonferoni corrected P value=0.0167
Theta (5-10Hz)	(2, N=48) =42, p<0.00001	(1, N=12) = 12, P<0.00054	(1, N=48) = 12, P<0.00054	(1, N=36) = 36, p<0.00001
Beta (15-35Hz)	(2, N= 38)~= 20.9, P<0.00025	(1, N=25)~= 21.2, p<0.00001	(1, N=37)~=3.27, P=0.070546 N.S.	(1, N=14)~=10.3, P=0.00134
Low Gamma (35-50Hz)	(2, N=23)~=4.52, P~=0.10 N.S.	(1, N=20) = 0.2, P~=0.65 N.S.	(1, N=12) = 3, P~=0.08 N.S.	(1, N=14)~= 4.57, P~= 0.03 N.S.
High Gamma (50-70Hz)	(2, N=41)~= 16.7, P<0.00023	(1, N=25) = 17.64, P<0.00003	(1, N=39)~= 1.26, P~=0.26 N.S.	(1, N=18) ~=10.9, P<0.00097
Very High Gamma (75-115Hz)	(2, N=49)~= 28.2, p<0.00001	(1, N=19) = 19, P=0.00001	(1, N=49)~= 2.47, P~=0.12 N.S.	(1, N=30) = 30, p<0.00001

Table 2b. **Chi Squared Tests for significant differences in proportion of putative inhibitory cells coherent to a given rhythm for a given condition. (N.S. not significant)**

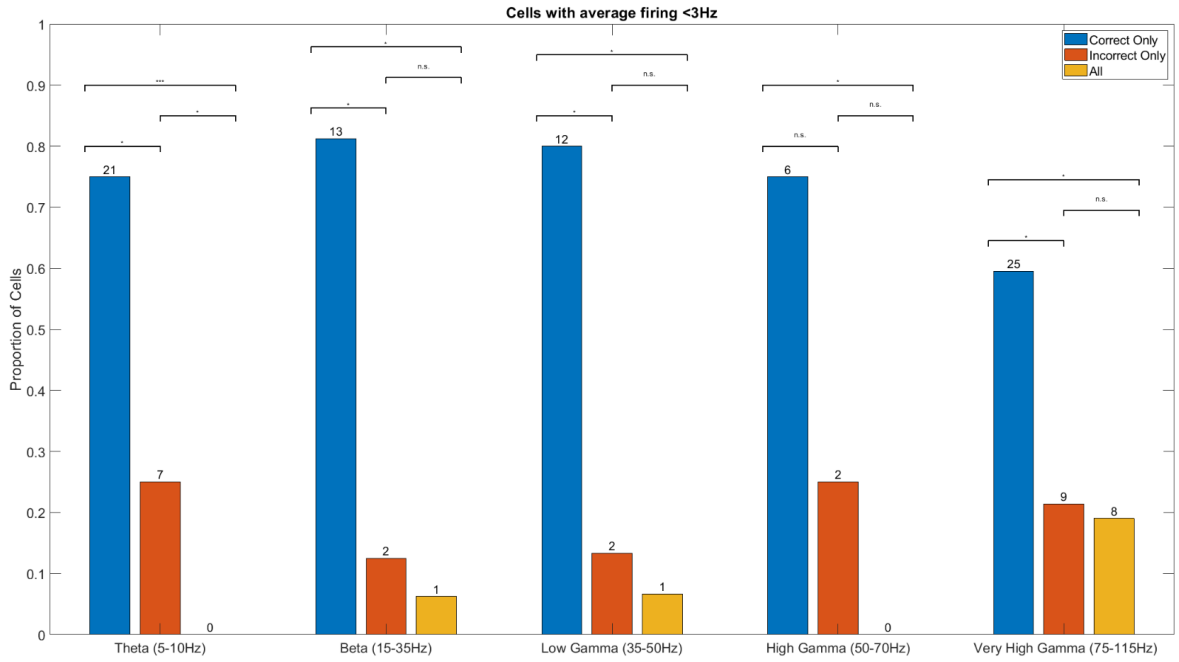

Figure 2a: **Proportion of putative granule cells which exhibited coherence to each rhythm of interest per outcome. (n.s. p=>0.0167; * p<=0.0166; ** p<=1E-3; *** p<=1E-4)**

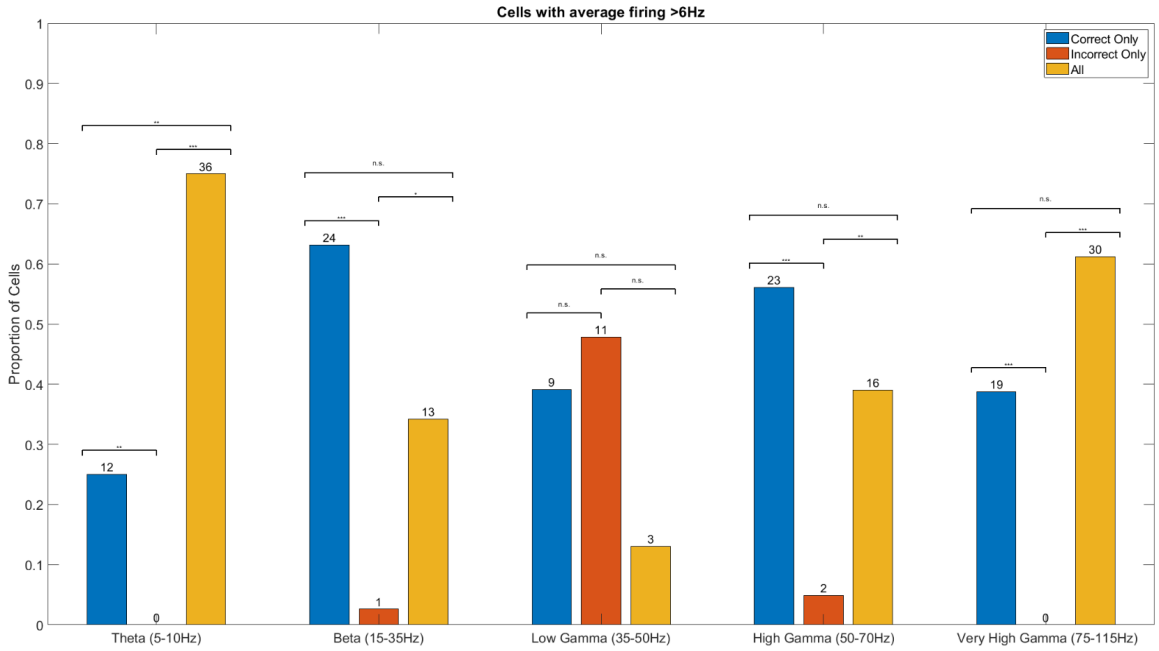

Figure 2b: **Proportion of putative inhibitory cells which exhibited coherence to each rhythm of interest per outcome. (n.s. p=>0.0167; * p<=0.0166; ** p<=1E-3; *** p<=1E-4)**

Effects of interval firing rate on validity of spike phase relationships

Since firing rates in phase-modulated cells can bias estimates of spike-phase coherence strength, we determined whether firing rate differences between correct and incorrect trials could explain the differences in selective coherence. No significant differences in nose poke interval firing rates could be observed between coherent putative granule cells during correct and incorrect trials (Fig 3a; Table 3 (left)). Thus

engagement by putative granule cells across outcomes was not biased by firing rate differences of the cells in each outcome.

In contrast, firing rates during nose poke intervals for putative inhibitory cells coherent to each respective rhythm of interest differed significantly across correct and incorrect outcomes (Fig 3b; Table 3 (right)). A decrease in coherence during an interval could be due to significantly lower firing rates during that interval. Of the putative inhibitory cells with beta coherence, a significantly greater proportion of cells were only coherent during correct trials. However, this 'correct only' population had a significantly lower interval average firing rate. Thus, the lack of inhibitory cell engagement during the nose poke interval associated with incorrect trials only is not a function of firing rate difference between the intervals. For the cells coherent to all other rhythms of interest, all populations exhibited the opposite trend, indicating the need for further investigation into the validity of the rayleigh statistic used to assess spike phase coherence.

Overall differences in interval firing rate between correct and incorrect trials

All putative granule cells and putative inhibitory interneurons which fired during either correct or incorrect intervals were pooled, then their firing rates were compared across cue intervals corresponding to correct and incorrect trials. Putative granule cells did not have a significantly different firing rate depending on the corresponding outcome (Wilcoxon signed rank test Z=-0.119 P=0.904 $\text{Median}_{\text{Correct}}$=0.0970, $\text{Median}_{\text{Incorrect}}$=0.0833). Putative inhibitory interneurons did

however, exhibit significantly different firing rates during the cue interval depending on the corresponding outcome, with a trend towards greater firing during incorrect trials (Z=-3.474, P=0.00051, $Median_{Correct}$=8.2758, $Median_{Incorrect}$=9.2182).

	Wilcoxon signed-rank test Correct Vs Incorrect Putative Granule cells (<3Hz)	Wilcoxon signed-rank test Correct Vs Incorrect Putative Inhibitory interneurons (>6Hz)
Theta (5-10Hz)	Z=-0.818, P~= 0.41 n.s.	Z=-3.705, P=0.00021, $Median_{Correct}$=8.7521, $Median_{Incorrect}$=10
Beta (15-35Hz)	Z=-1.206, P~=0.23 n.s.	Z=-3.589, P=0.00033, $Median_{Correct}$=8.5421, $Median_{Incorrect}$=10
Low Gamma (35-50Hz)	Z=N/A, P~=0.55 n.s.	Z=-3.220, P=0.00128, $Median_{Correct}$=8.8468, $Median_{Incorrect}$=10.9090
High Gamma (50-70Hz)	Z=-0.879, P~=0.38 n.s.	Z=-3.342, P=0.00082, $Median_{Correct}$=10.7508, $Median_{Incorrect}$=8.7364
Very High Gamma (75-115Hz)	Z=N/A, P~=0.36 n.s.	Z=-2.646 P=0.00814, $Median_{Correct}$=8.3636, $Median_{Incorrect}$=9.7142

Table 3. **Wilcoxon signed-rank test for significant differences in firing rate of cells coherent to each rhythm during nose poke intervals predicting correct or incorrect associative memory task performance. If a significant difference was found, median firing rate for each category was also reported.**

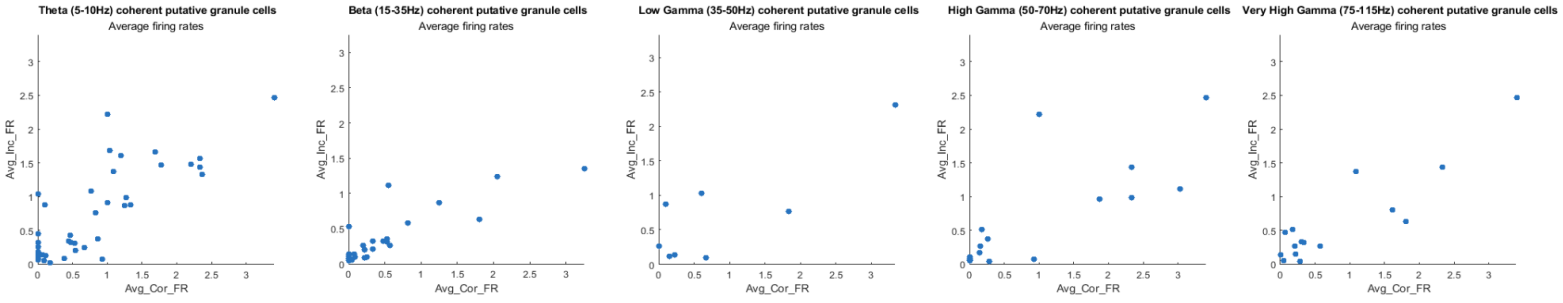

Fig 3a. **Average firing rate of coherent putative granule cells during nose poke intervals associated with correct trial vs those associated with incorrect trials, for each rhythm of interest, for neurons which exhibited significant spike phase relationships during either correct or incorrect trials.**

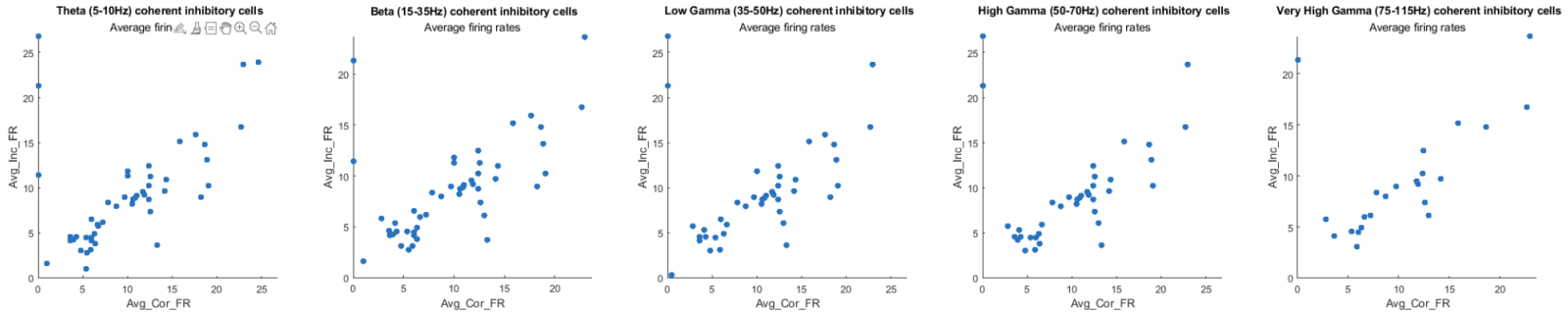

Fig 3b. **Average firing rate of putative inhibitory cells during nose poke intervals associated with correct trial vs those associated with incorrect trials, for each rhythm of interest, for neurons which exhibited significant spike phase relationships during either correct or incorrect trials.**

Discussion:

During the odor cue interval, we observed shifts in contribution of the multiple frequency bands to the local field potential: theta (5-10 Hz), beta (15-35 Hz), low gamma (35-50 Hz), high gamma (50-70 Hz) and very high gamma (75-115 Hz). These shifts could reflect the modulation of circuit activity during the cue interval. Further, as we observed cessation of these rhythmic signals with cessation of the odor cue prior to the reward interval, the circuits they may be reflective of engaging are likely to disentangle in function to those previously associated with reward consumption (Sasaki et al., 2018). We also observed modulation of two of these rhythmic signals in a manner predictive of associative memory performance.

Theta (5-10 Hz) and very high gamma (75-115 Hz) frequency bands' mean amplitude decreased during odor cue intervals which corresponded to correct performance on the associative memory task. Theta, and to a lesser extent gamma, hippocampal oscillations have previously been positively correlated with motor activity and indirectly related to associative memory processes (Trimper et al., 2017; Zheng et al., 2016; Ahmed & Mehta, 2012**).** However, decreases in theta power have also been independently associated with approaching a choice point associated with a potential reward outcome. As such, it has been suggested a decrease in theta is reflective of a behavioral state several 100ms in the future, and is a 'readiness signal' (Wyble et al., 2004). Other research has shown cue dependent decreases in theta coupled with increases in beta in response, regardless of the valence of the associated outcome.

Additionally, observed theta-beta interaction did not occur in response to cessation of movement alone (Rangel et al., 2015). While we did not find a unique increase in beta with the cessation of theta correlated with cue intervals which predicted correct associations, theta may have still acted as a 'readiness signal. Our results may indicate that this 'readiness signal' may be a scalable factor for the permission of neurons to engage in circuits crucial for mnemonic processing.

Some studies have suggested that very high gamma is generated by parvalbumin positive (PV+) inhibitory interneurons (Mann & Paulsen, 2007; Sohal et al., 2009; Towers et al., 2001**)**. Computational models of DG circuitry (Estarellas, 2016) suggest LTP along the preferent path (such as what may occur especially strongly with repetition of learned conjunctive object-spatial cues for an associative memory) could reduce activation of the PV+ inhibitory interneurons. It's possible that during exemplary associative memory processing of a given set of associative cues, a dentate circuit which had been previously modified --through the above steps-- for given these cues is reengaged, leading to a down regulation of PV+ interneurons and inturn, a downregulation of the very high gamma band. This aligns with our observed decreased firing rate of putative inhibitory interneurons during cue intervals which predicted correct trials. In contrast, we did not observe any significant differences in firing rate of putative granule cells. While the lack of outcome dependent firing rates in putative granule cells may decrease the plausibility of the hypothesis built on Estarellas 2016 model -- that stronger LTP from repeated sensory inputs on granule cells from repeated

experience of associative cues will induce changes in the circuit which ultimately lead to reduced feedforward inhibition, greater firing rates of putative granule cells, and improved associative memory processing -- more investigation is needed to determine relationship between what each putative granule cells specifically encoded and their firing rate changes. However, we did find dramatic differences in spike phase preferences of putative granule cells between correct and incorrect associative memory task performance.

For all rhythms besides high gamma, we observed a significantly greater proportion of putative granule cells exhibiting significant spike phase relationships during cue intervals corresponding to correct trials only. These results were not modulated by firing rate suggesting that when these putative granule cells fire may be drastically more important for associative memory processing than how often they fire. Thus, shifts in circuit dynamics of the dentate gyrus play a major role in associative memory processing.

Limitations:

While we are reasonably confident that the >6Hz population represented primarily inhibitory interneurons and the <3Hz population represented primarily granule cells, a less proportion of the 3Hz population may have also included mossy cells and to an even lesser extent, inhibitory interneurons. Literature on firing rate of each cell type is extremely limited and at times at odds with itself (Kim et al., 2020; Jung et al. 2019; Estarellas et al., 2019; Senzai & Buzuki, 2017). Without optogenetic and

histological techniques, we can not say for certain the structural cell types contained within each population.

Future directions:

It is possible that the convergence of multiple sensory inputs to single granule cells is responsible, in part, for our observed results. A conjunctive neural code which integrates each unique combination of sensory cues to predict a given outcome could be a powerful and efficient tool in our task. Such a code would be a powerful and efficient tool not just for associative memory, but also many of the other mnemonic processes frequently attributed to the DG (i.e. pattern separation (Aimone et al., 2011; Rangel et al., 2014; Leutgeb et al., 2007; Neunuebel & Knierim 2014), novelty detection (Dees and Kesner, 2013), binding (Lee & Jung, 2017; O'Reilly & Rudy, 2001;)). Put simply, it becomes easier to discriminate between sets of sensory information when all aspects of each experience are considered.

Similar temporal conjunctive encoding mechanisms have been observed in other hippocampal subregions such as CA1. For instance, Rangel and colleagues found CA1 beta coherent principal cells exclusively coded conjunctive information, as opposed to information about odor or position alone (Rangel et al, 2016). Considering how disruption of preforant paths from entorhinal cortices to DG but not other hippocampal subregions effects memory tasks that would benefit from such a code, its possible that DG generates a more distinctive conjunctive code from CA1 or that a proportion of conjunctions observable in CA1 originate in DG.

Furthermore, previously in vivo electrophysiological recordings in the rat DG have shown that single granule cells can demonstrate distinct firing rate patterns for similar spatial environments (Leutgeb et al., 2007; Neunuebel, J. P. & Knierim, J. J., 2014), and that distinct populations of active cells can encode temporal differences between environments (Rangel, L. M. et al., 2014). Similar events within a given spatiotemporal context or the same event in similar spatiotemporal contexts might then be represented very differently at the single cell level in DG through cells that are highly selective for specific event and context associations.

Mechanistically, the combined sensory inputs and unique circuitry of DG may be crucial for such a feat. Computational models (Estarellas, 2016), which have been supported by transgenic experiments and in vitro studies (Estarellas et al., 2019), suggest that as LTP occurs along the perforant path and between the DG cell types, a net depression of feed-forward inhibition is temporarily experienced by granular cells. This could lead to circuits exhibiting patterns of small, highly specific, temporal windows corresponding to decreased signal transduction of the parvalbumin (PV+) inhibitory interneurons, alterations in timing of granule cell firing, and a circuit which is more uniquely tuned to transmit their signal. Proximally timed inputs from the perforant pathways, driven by object spatial conjunctions, could stimulate granule cells with greatest intensity and thus direct the relatively large sums of LTP. Consequently, a positive feedback mechanism would engrain only the most temporally coordinated and commonly occurring non-spatial-spatial conjunctions. This would result in a highly

distinct set of conjunctions being encoded shifts in circuit dynamics, observable through spike phase relationships. Potentially, the same spike phase relationships we've identified in this study.

Further investigation into the potential of conjunctive encoding properties of the putative granule cells identified to exhibit spike phase relationships for correct outcomes will be the next step in testing these theoretical predictions.

Acknowledgements:

I'm in deep gratitude to all members of the Neural Crossroads Laboratory for their assistance in all steps of the analysis process and their guidance in understanding the behavior and physiology of the research animals. A special thanks to Dr. Lara Rangel, Mia Borezzelo, Pamela Riviere, and Austin Galleher. Additionally, I would like to thank Dr. Marta Kutas for her teachings on how to effectively present scientific findings.

	Pairwise Bonferroni Test Theta (5-10Hz)$_{\text{Correct Vs Incorrect}}$	Pairwise Bonferroni Test Very High Gamma (75-115Hz)$_{\text{Correct vs Incorrect}}$
0-250ms from nose poke	d.f.=175, t=1.52989, p=1 n.s.	d.f.=175, t=0.18626, p=1 n.s.
250-500ms from nose poke	d.f.=175, t=1.37543, p=1 n.s.	d.f.=175, t=0.1012, p=1 n.s.
500-750ms from nose poke	d.f.=175, t=2.18286, p=1 n.s.	d.f.=175, t=1.55124, p=1 n.s.
750-1000ms from nose poke	d.f.=175, t=2.18286, p=1 n.s.	d.f.=175, t=1.55124, p=1 n.s.
1000-1250ms from nose poke	d.f.=175, t=2.44537, p=1 n.s.	d.f.=175, t=2.53616, p=1 n.s.
1250-1500ms from nose poke	d.f.=175, t=2.26631, p=1 n.s.	d.f.=175, t=1.75791, p=1 n.s.

S1. **Pairwise statistics examining interaction effects for each time bin following initiation of the odor sampling interval**

References

Ahmed, O. J., & Mehta, M. R. (2012). Running speed alters the frequency of hippocampal gamma oscillations. The Journal of neuroscience : the official journal of the Society for Neuroscience, 32(21), 7373–7383. https://doi.org/10.1523/JNEUROSCI.5110-11.2012

Aimone, J. B., Deng, W., & Gage, F. H. (2011). Resolving New Memories: A Critical Look at the Dentate Gyrus, Adult Neurogenesis, and Pattern Separation. Neuron, 70(4), 589–596. https://doi.org/10.1016/j.neuron.2011.05.010

Amaral, D. G., Scharfman, H. E., & Lavenex, P. (2007). The dentate gyrus: fundamental neuroanatomical organization Progress in brain research, 163, 3–22. https://doi.org/10.1016/S0079-6123(07)63001-5

Bibbig, A., Traub, R. D., and Whittington, M. A. (2002). Long-range synchronization of gamma and beta oscillations and the plasticity of excitatory and inhibitory synapses: a network model. J. Neurophysiol. 88, 1634–1654. doi: 10.1152/jn.00064.2002

Buckmaster, P. S., & Schwartzkroin, P. A. (1995). Interneurons and inhibition in the dentate gyrus of the rat in vivo. Journal of Neuroscience, 15(1 II), 774–789. https://doi.org/10.1523/jneurosci.15-01-00774.1995

Buzsáki G. (2010). Neural syntax: cell assemblies, synapsembles, and readers. Neuron, 68(3), 362–385. https://doi.org/10.1016/j.neuron.2010.09.023

Cannon, J., McCarthy, M. M., Lee, S., Lee, J., Börgers, C., Whittington, M. A., & Kopell, N. (2014). Neurosystems: brain rhythms and cognitive processing. The European journal of neuroscience, 39(5), 705–719. https://doi.org/10.1111/ejn.12453

Dees, R.L., Kesner, R.P., The role of the dentate gyrus in object and object-context recognition, Neurobiol. Learn. Mem. 106 (2013) 112–117.

Eichenbaum, Howard (2015). The advantages of large scale neural recording: Revealing the organization and dynamics of cognitive maps. [Conference presentation]. Society for Neuroscience 2015, Chicago, IL, United States. https://youtu.be/8GiFY8As9Mg

Estarellas, C., Mirasso, C. R., & Canals Gamoneda, S. (2019). Inhibitory Gating in the Dentate Gyrus. http://hdl.handle.net/10261/218196

Estarellas, C. M. (2016). Modeling the Entorhinal Cortex - Dentate Gyrus Circuit [UNIVERSITAT DE LES ILLES BALEARS]. https://ifisc.uib-csic.es/media/publications/publication/vyrBqjjXQ5elA0bkQJ3XzA.pdf\

Fernández-Ruiz, A., & Oliva, A. (2016). Distributed representation of “what” and “where” information in the parahippocampal region. Journal of Neuroscience, 36(32), 8286–8288. https://doi.org/10.1523/JNEUROSCI.1581-16.2016

Hunsaker, M. R., Mooy, G. G., Swift, J. S., & Kesner, R. P. (2007). Dissociations of the Medial and Lateral Perforant Path Projections Into Dorsal DG, CA3, and CA1 for Spatial and Nonspatial (Visual Object) Information Processing. Behavioral Neuroscience, 121(4), 742–750. https://doi.org/10.1037/0735-7044.121.4.742

Jung, D., Kim, S., Sariev, A., Sharif, F., Kim, D., & Royer, S. (2019). Dentate granule and mossy cells exhibit distinct spatiotemporal responses to local change in a one-dimensional landscape of visual-tactile cues. Scientific reports, 9(1), 9545. https://doi.org/10.1038/s41598-019-45983-6

Kesner, R. P. (2018). An analysis of dentate gyrus function (an update). Behavioural Brain Research, 354(February 2017), 84–91. https://doi.org/10.1016/j.bbr.2017.07.033

Kim, S., Jung, D., & Royer, S. (2020). Place cell maps slowly develop via competitive learning and conjunctive coding in the dentate gyrus. Nature Communications, 11(1), 1–15. https://doi.org/10.1038/s41467-020-18351-6

Kopell, N., Ermentrout, G. B., Whittington, M. A., and Traub, R. D. (2000). Gamma rhythms and beta rhythms have different synchronization properties. Proc. Natl. Acad. Sci. U.S.A. 97, 1867–1872. doi: 10.1073/pnas.97.4.1867

Kopell, N., Kramer, M. A., Malerba, P., & Whittington, M. A. (2010). Are different rhythms good for different functions? Frontiers in Human Neuroscience, 4(November), 1–9. https://doi.org/10.3389/fnhum.2010.00187

Lee, J. W., & Jung, M. W. (2017). Separation or binding? Role of the dentate gyrus in hippocampal mnemonic processing. Neuroscience and Biobehavioral Reviews, 75, 183–194. https://doi.org/10.1016/j.neubiorev.2017.01.049

Leutgeb, J. K., Leutgeb, S., Moser, M. B., & Moser, E. I. (2007). Pattern separation in the dentate gyrus and CA3 of the hippocampus. Science (New York, N.Y.), 315(5814), 961–966. https://doi.org/10.1126/science.1135801

Mitra P., Bokil H. (2008). Observed Brain Dynamics Observed. Brain Dynamics: Oxford University

Morris, A. M., Weeden, C. S., Churchwell, J. C., & Kesner, R. P. (2013). The role of the dentate gyrus in the formation of contextual representations. Hippocampus, 23(2), 162–168. https://doi.org/10.1002/hipo.22078

Neunuebel, J. P., & Knierim, J. J. (2014). CA3 retrieves coherent representations from degraded input: direct evidence for CA3 pattern completion and dentate gyrus pattern separation. Neuron, 81(2), 416–427. https://doi.org/10.1016/j.neuron.2013.11.017

O'Reilly, R. C., & Rudy, J. W. (2001). Conjunctive representations in learning and memory, principles of cortical and hippocampal function. Psychological Review, 108, 311–345.

Pinto, D. J., Jones, S. R., Kaper, T. J., and Kopell, N. (2003). Analysis of state-dependent transitions in frequency and long-distance coordination in a model oscillatory cortical circuit. J. Comput. Neurosci. 15, 283–298. doi: 10.1023/A:1025825102620

O'Reilly, R. C., & Rudy, J. W. (2001). Conjunctive representations in learning and memory, principles of cortical and hippocampal function. Psychological Review, 108, 311–345.

Rangel, L. M., Alexander, A. S., Aimone, J. B., Wiles, J., Gage, F. H., Chiba, A. A., & Quinn, L. K. (2014). Temporally selective contextual encoding in the dentate gyrus of the hippocampus. Nature Communications, 5(1), 3181. https://doi.org/10.1038/ncomms4181

Rangel, L., Chiba, A., & Quinn, L. (2015). Theta and beta oscillatory dynamics in the dentate gyrus reveal a shift in network processing state during cue encounters . In Frontiers in Systems Neuroscience (Vol. 9, p. 96). https://www.frontiersin.org/article/10.3389/fnsys.2015.00096

Rangel, L. M., Rueckemann, J. W., Riviere, P. D., Keefe, K. R., Porter, B. S., Heimbuch, I. S., Budlong, C. H., & Eichenbaum, H. (2016). Rhythmic coordination of hippocampal neurons during associative memory processing. ELife, 5. https://doi.org/10.7554/eLife.09849

Rolls, E.T. (1996), A theory of hippocampal function in memory. Hippocampus, 6: 601-620. https://doi.org/10.1002/(SICI)1098-1063(1996)6:6<601::AID-HIPO5>3.0.CO;2-J

Sasaki, T., Piatti, V. C., Hwaun, E., Ahmadi, S., Lisman, J. E., Leutgeb, S., & Leutgeb, J. K. (2018). Dentate network activity is necessary for spatial working memory by supporting CA3 sharp-wave ripple generation and prospective firing of CA3 neurons. Nature neuroscience, 21(2), 258–269. https://doi.org/10.1038/s41593-017-0061-5

Senzai, Y., & Buzsáki, G. (2017). Physiological Properties and Behavioral Correlates of Hippocampal Granule Cells and Mossy Cells. Neuron, 93(3), 691–704.e5. https://doi.org/10.1016/j.neuron.2016.12.011

Sohal, V. S., Zhang, F., Yizhar, O., & Deisseroth, K. (2009). Parvalbumin neurons and gamma rhythms enhance cortical circuit performance. Nature, 459(7247), 698–702. https://doi.org/10.1038/nature07991

Towers, S. K., LeBeau, F. E., Gloveli, T., Traub, R. D., Whittington, M. A., & Buhl, E. H. (2002). Fast network oscillations in the rat dentate gyrus in vitro. Journal of neurophysiology, 87(2), 1165–1168. https://doi.org/10.1152/jn.00495.2001

Trimper, J. B., Galloway, C. R., Jones, A. C., Mandi, K., & Manns, J. R. (2017). Gamma Oscillations in Rat Hippocampal Subregions Dentate Gyrus, CA3, CA1, and Subiculum Underlie Associative Memory Encoding. Cell reports, 21(9), 2419–2432. https://doi.org/10.1016/j.celrep.2017.10.123

Verret, L., Mann, E. O., Hang, G. B., Barth, A. M., Cobos, I., Ho, K., Devidze, N., Masliah, E., Kreitzer, A. C., Mody, I., Mucke, L., & Palop, J. J. (2012). Inhibitory interneuron deficit links altered network activity and cognitive dysfunction in Alzheimer model. Cell, 149(3), 708–721. https://doi.org/10.1016/j.cell.2012.02.046

Wyble, B. P., Hyman, J. M., Rossi, C. A., & Hasselmo, M. E. (2004). Analysis of theta power in hippocampal EEG during bar pressing and running behavior in rats during distinct behavioral contexts. Hippocampus, 14(5), 662–674. https://doi.org/10.1002/hipo.20012

Zheng, C., Bieri, K. W., Hwaun, E., & Colgin, L. L. (2016). Fast Gamma Rhythms in the Hippocampus Promote Encoding of Novel Object-Place Pairings. eNeuro, 3(2), ENEURO.0001-16.2016. https://doi.org/10.1523/ENEURO.0001-16.2016